Nickel addition to optimize the hydrogen storage performance of lithium intercalated fullerides

Nickel Addition to Optimize the Hydrogen Storage performance of Lithium Intercalated Fullerides

Matteo Aramini[1,2], Giacomo Magnani[2], Daniele Pontiroli[2,*],Chiara Milanese[3,*], Alessandro Girella[3], Giovanni Bertoni[4,5], Mattia Gaboardi[2,6], Stefano Zacchini[7], Amedeo Marini[3], Mauro Riccò[1]

[1]*Diamond Light Source, Harwell Science & Innovation Campus, Didcot, Oxfordshire, OX11 0DE, UK*

[2] *Nanocarbon Laboratory, Dipartimento di Scienze Matematiche, Fisiche e Informatiche, Università degli studi di Parma, Parco Area delle Scienze 7/A, 43124 Parma, Italy*

[3] *Pavia H_2 Lab, C.S.G.I & Dipartimento di Chimica, Sezione di Chimica Fisica, Università degli Studi di Pavia, Viale Taramelli 16, 27100 Pavia, Italy*

[4] *IMEM-CNR, Parco Area delle Scienze 37/A, 43124 Parma, Italy*

[5] *CNR - Istituto Nanoscienze, Via Campi 213/A, I-41125 Modena, Italy*

[6] *Elettra Sinctrotrone Trieste SCpA, Parco Area Science SS14, Km. 163.5, I-34012, Basovizza, Italy*

[7] *Dipartimento di Chimica Industriale, Università di Bologna, Viale del Risorgimento, 4, Bologna, Italy*

Abstract:

The addition of transition metals to alkali intercalated fullerides proved to enhance their already good hydrogen absorption properties. Herein we present a study based on two different synthetic strategies, allowing the addition of nickel as aggregates with different size to the lithium fulleride Li_6C_{60}: the former is based on the metathesis of nickel chloride, while the latter on the thermal decomposition of nickel carbonyl clusters. The hydrogen-storage properties of the obtained materials have been investigated with manometric and calorimetric measurements, which indicated a clear enhancement of the final absorption value and kinetics with respect to pristine Li_6C_{60}, as a consequence of nickel surface catalytic activity towards hydrogen molecules dissociation. We found up to 10% increase of the total H_2 weight % absorbed (5.5 wt% H_2) in presence of Ni aggregates. Furthermore, the control of the transition metal particles size distribution allowed to reduce the hydrogen desorption enthalpy of the systems.

Keywords: hydrogen-storage, transition metal decoration, lithium fullerides, nickel nanoparticles.

[*]Corresponding author: Daniele Pontiroli, Dipartimento di Scienze Matematiche, Fisiche e Informatiche, Università degli studi di Parma, Parco Area delle Scienze 7/A, 43124 Parma, Italy. E-mail: daniele.pontiroli@unipr.it.

1. Introduction

Carbon-based nanostructured materials, such as fullerenes and graphene, play a key role in the field of energy generation, distribution and storage [1, 2]. Thanks to their unusual physical properties, their scalable production at the industrial level and their intrinsic biocompatibility, carbon nanomaterials naturally fulfill many of the needed requirements; either for the development of versatile renewable carbon-based energy sources [3], or for their possible use in smart distribution networks, thanks to their employment as components (electrodes, solid electrolytes or membranes) in electrochemical accumulators, supercapacitors and fuel cells [4-9]. Moreover, their possible use in efficient solid-state hydrogen-storage systems has also been widely investigated [10].

In particular, the high specific surface of graphene (2630 m^2/g) allows large H_2 amounts to be physically adsorbed at 77 K [11], and the performance can be even enhanced by decorating it with transition metals [12, 13]. Also hydrogen chemical absorption is possible on the graphene plane, where sp^2 C atoms can be converted into a sp^3 hybridization giving graphane, in which up to 7.7 wt% of H_2 can be ideally stored [14]. Chemical absorption seems not to prevent the H local diffusion on graphene [15, 16]**,** and also H_2 absorption via spillover effect was recently observed in graphenic systems [17].

According to recent theoretical predictions, hydrogen interaction with carbon can be increased if sp^2 carbon layers are curved [18] and charged [19], conditions which are naturally met in the alkali intercalated fullerenes (so-called "fullerides"). In fact, many theoretical forecasts identified alkali metals decorated fullerenes as ideal systems for room temperature reversible H_2 storage [20], since they are expected to bind hydrogen molecules through orbital interactions [21] and therefore with relatively low reaction enthalpy. However, experimental results showed that alkali do not decorate C_{60}, but they prefer to intercalate as small clusters into the voids of the *fcc* fullerene lattice [22, 23]. Nevertheless, an efficient H_2 absorption was indeed confirmed in these compounds: Li_6C_{60}, $Li_{12}C_{60}$ and $Na_{10}C_{60}$ reversibly absorb relatively high H_2 amount, respectively 5, 4.5 and 3 wt% H_2 [24-26]. In these systems, the absorption process has been identified as driven via H_2 dissociation, mediated by the intercalated metal clusters, leading to the formation of chemical bonds between hydrogen atoms and the charged C_{60}^{n-} molecules [25, 27, 28], rather than to a quantum interaction of the H_2 molecule with the decorated fullerene. It is worth noting that also indirect up to 5.5 wt % hydrogen uptake has been reported in these systems, through a reversible solid-state ammonia-storage mechanism [29].

In muon spin relaxation (μSR) experiments on intercalated fullerides [30, 31], we succeeded to study separately the two absorption steps: 1) the initial molecular hydrogen dissociation

accomplished by the intercalated clusters and 2) the successive atomic H binding on the carbon backbone. These findings suggested that atomic H decoration of charged fullerides was identified as a spontaneous process, already active at 5 K. The relatively high temperatures (higher than 250°C) requested for the hydrogenation of these materials has been ascribed to the catalytic H_2 dissociation process mediated by the intercalated alkali metal clusters and hence represents a limiting factor for possible practical applications of these systems.

Many transition metals show catalysis towards H_2 splitting (see [32] and references therein); we identified the insertion of "*d"*-block elements aggregates and particles as a strategy aimed to low H_2 dissociation temperatures. Platinum (Pt) and palladium (Pd) addition to lithium intercalated fullerides has been demonstrated to be effective in the enhancement of the final uptake values and reaction kinetic [33]. Moreover, this study suggested an optimal transition metal (TM) stoichiometry, which corresponds to $Li_6TM_{0.11}C_{60}$ irrespective of the metal used.

In this manuscript, we present the addition of nickel (Ni) aggregates, obtained following two distinct synthetic routes, to lithium fullerides. We found that the presence of Ni clusters, similarly to what observed with Pt and Pd, leads to a significant improvement of the hydrogen absorption properties with respect to the fullerene-based material, either in term of absolute uptake value, or in term of kinetics. Furthermore, the control over the Ni particle size provides destabilization of hydrofullerene molecules, thus controlling the de-hydrogenation enthalpy. The hydrogen storage properties were explored with manometric and calorimetric measurements, while the morphology of the samples and their structural evolution was probed by powder X-ray diffraction, scanning and transmission electron microscopy.

2. Experimental

In order to prepare $Li_6Ni_{0.11}C_{60}$, two synthetic procedures have been developed. The former (Sample A) is based on mixing nickel chloride with Li_6C_{60} powder. C_{60} powder (MER 99.9%, further purified in vacuum at 250°C for 12 hours) and lithium metal (Sigma Aldrich, 99%, which was previously cut in small pieces) were mixed in a high-energy ball milling agate jar (Mini-mill Pulverisette23 – Fritsch, 10 ml volume, 3 agate spheres with 10 mm diameter each) at 30 Hz frequency for 10 minutes. A stoichiometric amount of $NiCl_2$ (Sigma Aldrich, 98%) was added to the as obtained Li_6C_{60} and the powders were further milled at 30 Hz frequency in two turns 10 minutes long, separated by 5 minutes pause, to prevent the ball milling overheating.

In the second synthesis, Li_6C_{60} was obtained by mixing lithium metal and C_{60} in an agate ball milling jar with high energy milling at 30 Hz frequency for three turns, 10 minutes each, separated

by 5 minutes intermission, as described elsewhere [33]. Two nickel-carbonyl clusters salts were used as Ni source: $[NBu_4]_2^+[Ni_6(CO)_{12}]^{2-}$ (Sample B1) and $[NEt_4]_3^+[HNi_{12}(CO)_{21}]^{3-}$ (Sample B2) respectively [34]. They were added to Li_6C_{60} powders by manual grinding for 15 minutes. Nickel cluster quantities were selected to provide a $Li_6Ni_{0.11}C_{60}$ final stoichiometry.

Thermal decomposition of the metal-carbonyl compounds can be obtained with a thermal annealing at mild conditions and was directly realized during the manometric heating ramp of absorption measurements, in order to provide Ni clusters directly at the hydrogenation step. The air sensitivity of all the samples required their handling and conservation under strict oxygen and moisture free condition in a pure Ar filled glove box, ensuring O_2 and H_2O contents lower than 1 ppm.

Hydrogenation studies were performed in the PCTPro-2000 manometric instrument by Hy-Energy &Setaram by heating the samples (about 200 mg each) from room temperature to 350°C at 5°C/min under 100 bar H_2 and appending an isotherm of 10 h. Discharged powders were analyzed by coupled calorimetric – manometric measurements by connecting the PCTPro to the Setaram Sensys high pressure Differential Scanning Calorimetry (DSC) cells with stainless steel high pressure tubes, in order to obtain the thermodynamic features of the desorption reactions [33, 35-37]. The charged powders (about 20 mg) were heated from room temperature up to 380°C under 0.5 bar H_2 at 5°C/min ramp and the kinetic and calorimetric signals were recorded simultaneously.

Scanning electron microscopy (SEM) was performed (without gold sputtering) on a Zeiss EVO®-MA10-HR microscope. To avoid air exposition of the samples, a home-made sample holder allowing the transfer of the samples from the glove-box in the SEM analysis chamber under vacuum has been used. The composition of the samples was determined by Energy-dispersive X-ray spectroscopy (EDS), using an INCA Energy 350 X Max detector from Oxford Instruments, equipped with a Be window. Cobalt standard was used for the calibration of the quantitative elementary analysis.

Powder X-Ray diffraction analysis (PXRD) was performed with Bruker D5005 and D8-Advance diffractometers (Cu Kα radiation) by using a suitable, sealed zero background sample holder on the first instrument and sealed capillaries on the second. The measurements conditions were: $5° \leq 2\theta \leq 60°$, step size 0.2°; 40 s for step; cathode voltage and current of 40 kV and 40 mA.

Transmission Electron Microscopy (TEM) analysis was performed with the dispersion of a small amount of sample in isopropanol in air. The suspension was sonicated for a minute and a droplet was deposited onto a carbon coated copper grids. High Angle Annular Dark Field (HAADF) Scanning Transmission Electron Microscopy (STEM) analyses were carried out on a JEOL JEM-2200FS microscope equipped with a Schottky gun operating at 200 kV and an Energy Dispersive

X-ray Spectroscopy (EDS) detector (JEOL JED-2300). STEM was carried out with a nominal probe size of 0.5 nm and an inner detector cut-off angle of about 75 mrad (HAADF).

3. Results and Discussion

3.1 $Li_6Ni_{0.1}C_{60}$ obtained from $NiCl_2$ salt

3.1.1. Calorimetric – Manometric measurements

Sample A shows a final absorption value **(at the end of the isothermal stage)** of 5.5 wt% of H_2 reached with a kinetics of $5.27 \cdot 10^{-2}$ wt%/min, as shown in Figure 1. Concerning kinetics, about 3.5 wt% H_2 is absorbed during the heating ramp and a content of 5 wt% H_2 is reached in 200 min. **This same value is reached at the end of the 80 min desorption ramp, testifying the reversibility of the hydrogenation – dehydrogenation processes.**

The DSC de-hydrogenation profile (shown in Figure 1 inset) shows the onset of an endothermic signal at 304°C which is formed by the overlapping of two very close peaks at 326°C and 338°C respectively. The related de-hydrogenation enthalpy value is 62.4 kJ/mol H_2. As a comparison, pure lithium intercalated fulleride Li_6C_{60} [33] shows a final uptake value of 5 wt% H_2 and an absorption rate in the order of $4.30 \cdot 10^{-2}$ wt%/min, indicating that the addition of the Ni salt to the intercalated structure allowed to sensitively improve the absorption performances. **In fact, it is well known from literature the role of Ni nanoparticles in facilitating the dissociative chemisorption of hydrogen molecules via the so-called "spillover effect" [38-41].**

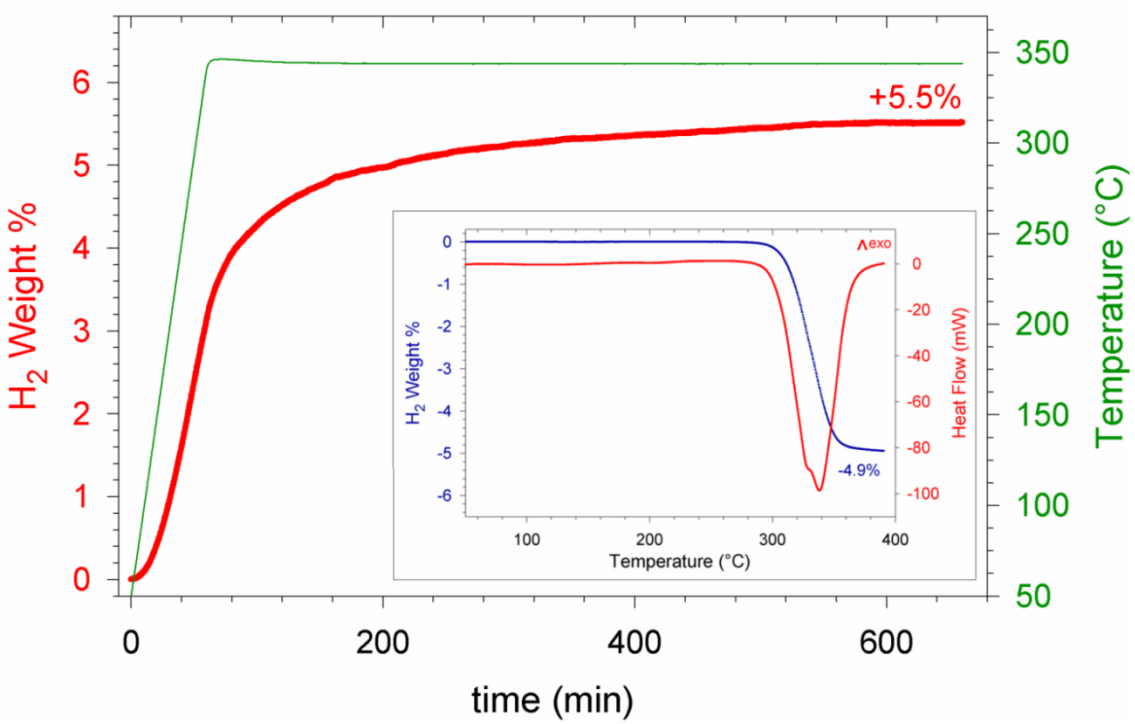

Figure 1: Kinetic absorption curve for sample A, obtained from the addition of nickel chloride (thick line). The temperature ramp profile is also reported (thin line). *Inset*: coupled manometric–calorimetric desorption profiles.

On the other hand, the de-hydrogenation enthalpy is similar to the one observed in pristine Li_6C_{60}, where the desorption onset is found at 306 °C and main peaks are at 326 °C and 336°C [32], thus suggesting that the same H desorption mechanisms should drive the de-hydrogenation process in pure and Ni-added samples.

3.1.2 Powder X-ray diffraction

XRD was performed on both pristine and hydrogenated sample A and is reported in figure 2. In the as-prepared sample (upper black pattern in Figure 2) the Li_6C_{60} phase accounts for the most intense peaks in the range 2θ = 10-40°. Peaks of this phase appear broad, indicating poor crystallization, but they can be indexed with the *fcc* cell (a= 14.15 Å, space group $Fm\bar{3}m$) of the monomer phase belonging to the lithium intercalated fulleride [42, 43]. A small fraction of the monoclinic phase isostructural to Li_4C_{60} polymer [44] is found as well in the pristine sample. Nevertheless, the temperature reached during the hydrogenation isotherm is expected to promote a transition from the polymer phase of lithium fulleride to its monomer $Fm\bar{3}m$ phase [42], thus indicating that the single monomer phase should undergo the H_2 treatment.

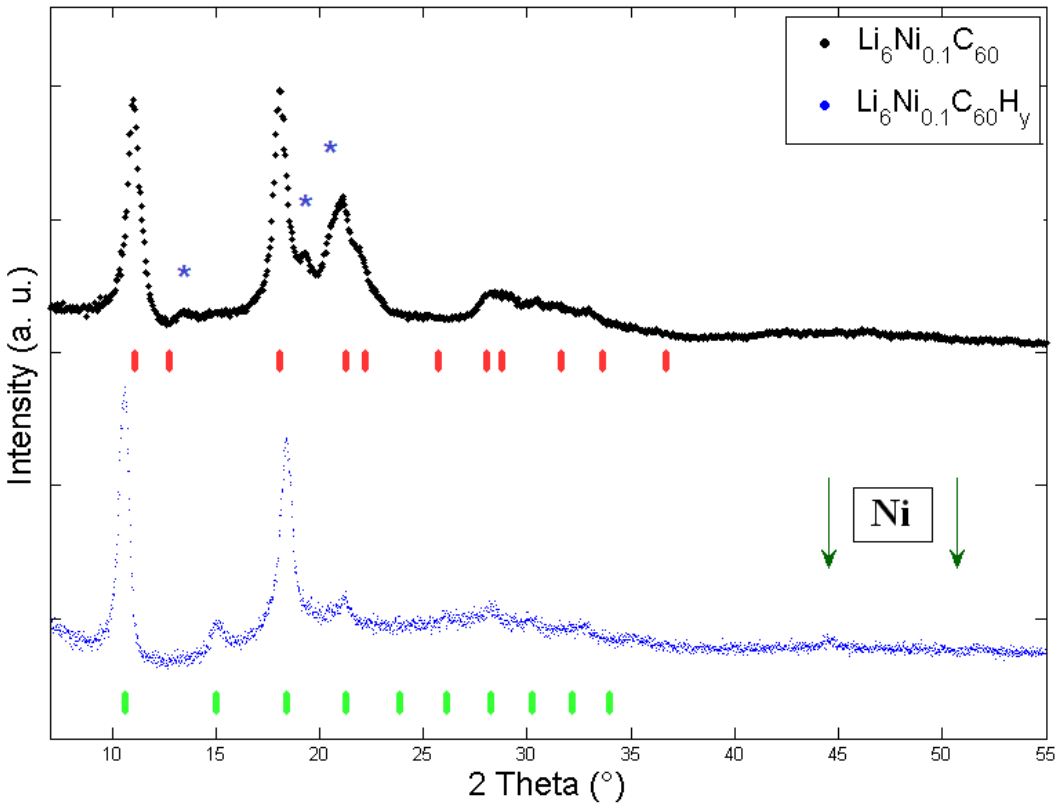

Figure 2: PXRD of as-prepared (upper dots) and hydrogenated (lower dots) sample A. Solid marks denote the positions of reflections belonging to *fcc* Li_6C_{60} (upper marks) and to the *bcc* hydrofulleride phase (lower marks). Arrows identify pure nickel reflections**, while the asterisks evidence the reflections ascribable to the monoclinic phase isostructural to Li_4C_{60}, present in pristine Li_6C_{60} sample.**

After the treatment under hydrogen (100 bar) at 350°C (patterns at the bottom of Figure 2), the majority of the sample takes a *bcc* crystalline arrangement (a = 11.85(4) Å, space group $Im\bar{3}m$), which is commonly observed in hydrofullerenes $C_{60}H_y$ [45]. In fact, the loss of the C_{60} I_h icosahedral symmetry and the increased steric hindrance of $C_{60}H_y$ make the *bcc* arrangement energetically more favorable than the *fcc* structure. The weak reflection at $2\theta = 44.50(6)°$ seems to suggest the presence of nickel metal consequent to the decomposition of $NiCl_2$.

3.1.3. Electron Microscopy

SEM images were collected in secondary and back scattered electrons modes and are reported in Figure 3 for pristine sample A (panels a and b, respectively) and for the sample A after hydrogenation (panels c and d, respectively). As-prepared sample A is composed by aggregates

characterized by a very broad size distribution: smaller particles have sub-micrometer dimensions, while largest ones reaches up to 30 μm diameter. After H_2 absorption, the particle mean dimensions seem to be finer than in pristine condition; even if agglomerates are still found, whose size is the same of pristine powder, the number of the smallest particles is increased, suggesting the aggregate fragmentation consequent to the heat treatment. Some brighter particles are clearly detected, on both pristine and treated sample, in backscattered electron images (panels b, d, Figure 3). These particles size is up to around 10 μm in the former case, while a noticeable reduction is found after hydrogenation, where the powders are only few **microns** sized.

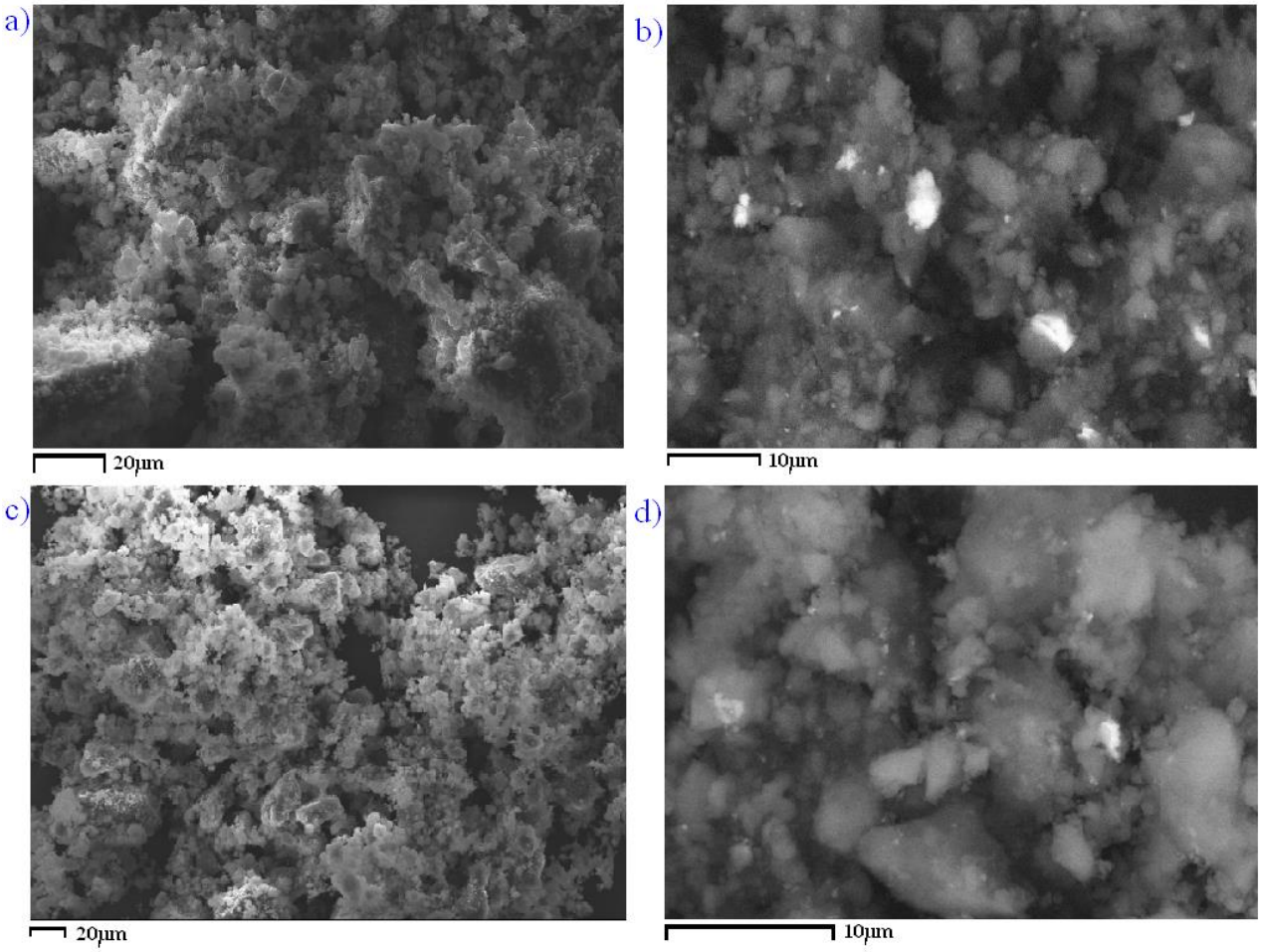

Figure 3: SEM secondary and backscattering electrons images of sample A, either in pristine form (panels a and b), or after hydrogen treatment (panels c and d).

EDS was used to investigate the $NiCl_2$ status in the sample and detected the conservation of the overall Ni/Cl atomic ratio in both as-prepared and H_2-treated sample conditions. This outcome guarantees no chlorine is released as HCl during the treatment under hydrogen.

In order to better probe the metal-chloride decomposition, we explored morphological and chemical composition with the smaller electron probe possessed by STEM in HAADF mode. This technique was used for its high contrast (roughly proportional to the square of atomic number of the elements in the sample), making possible to reveal small Ni particles in the thick carbon matrix. Many nanometer sized particles have been found in the range 2 – 50 nm often accumulated in relatively limited space regions (see Figure 4). Such a Ni particle arrangement can be explained by considering the decomposition of $NiCl_2$ precursor, which is introduced in the system with high energy ball milling. $NiCl_2$ decomposes at high temperatures, providing feed of the transition metal. Ni nucleation leads to formation of nanoparticles which are not homogeneously distributed in the fulleride matrix, but mainly concentrated in the limited regions previously occupied by the metal chloride crystals.

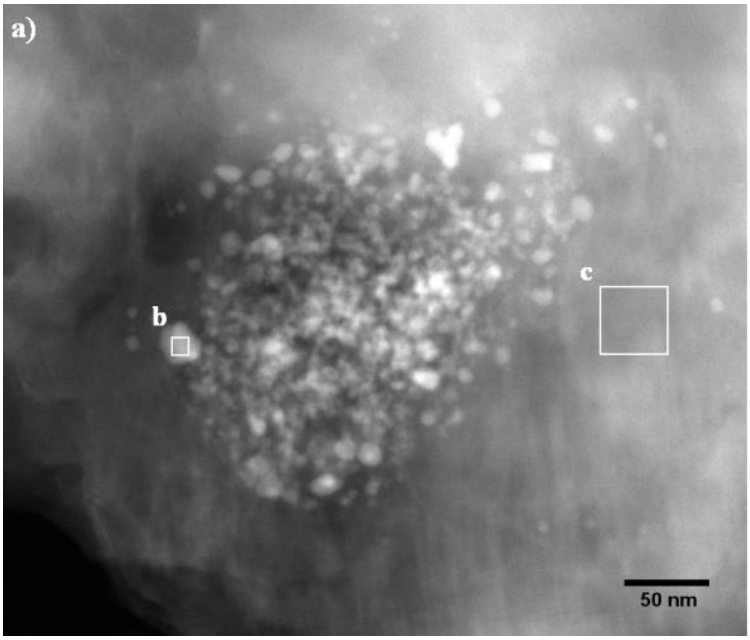

	Region (b)	Region (c)
Ni	99.5(1)	80.7(1)
Cl	0.5(1)	19.3(1)

Figure 4: On the left: HAADF-STEM picture of nickel nanosized particles in sample A after the hydrogenation process (a). On the right: elemental composition (atomic %) of sample A after the hydrogenation process, estimated with EDS analysis, on the nickel particle (b) and in the bulk region (c) respectively. Errors are expressed in brackets and the collection region are identified with light marks.

This was also confirmed by energy dispersive spectroscopy study, shown in figure 4. On a 40x40 nm carbon region the atomic percentage of Ni and Cl is 80.7 and 19.3, respectively. The single particle, on the contrary, is essentially composed by nickel and only a small Cl fraction can be detected (Ni: 99.5, Cl: 0.5 atomic %).

Stronger peaks belonging to carbon, oxygen, and copper were detected also with EDS (red colored in spectra in figure 1S): the first is naturally present as main component of our samples. Copper

arises from the grid used for suspending the sample, while the presence of oxygen is due to contamination during short exposure of samples to air before the STEM measurements.
These findings suggest $NiCl_2$ decomposition according to the metathesis reaction:

$$Li_6C_{60} + 0.1\ NiCl_2 \rightarrow Li_{5.8}C_{60} + 0.1\ Ni + 0.2\ LiCl, \qquad [1]$$

which is accomplished at 350°C under 100 bar H_2 and where chlorine reacts with lithium forming small amount of LiCl salt, providing the Cl fraction detected on the fulleride matrix.
A small Cl signal is detected on the particles also, probably arising from LiCl present in the underlying zones supporting the particles; however, the predominance of Ni in individual particles(far higher atomic percentage than in $NiCl_2$) shows that the hydrogenation treatment (100 bar H_2 at 350 °C) provided the salt decomposition and the release of pure nickel in the sample. Micrometer sized particles shown by SEM study were not found in TEM, probably as a consequence of powder dispersion in the solvent during TEM sample handling.
Even if heat treatment condition was milder than the one required for $NiCl_2$ decomposition[46], the described synthesis releases transition metal particles with a broad distribution, ranging from few nm to μm-sized aggregates, during the heat treatment under H_2.

3.2 $Li_6Ni_{0.1}C_{60}$ obtained from nickel molecular clusters

3.2.1 Calorimetric – Manometric measurements

Sample B1 and B2 reached a final absorption value of 5.2 wt% H_2 and 5.5 wt% H_2, respectively. The absorption curve of the former compound is shown in Figure 5: around 3.5 wt% H_2 was stored during the initial ramp and an uptake of 5 wt% H_2 was obtained after 6 hours of the isothermal stage. The latter, whose manometric kinetic measurements are reported in Figure 6, absorbed 3.5 wt% H_2 in the initial heating and reached 5 wt% H_2 after only 3 hours at 350°C.

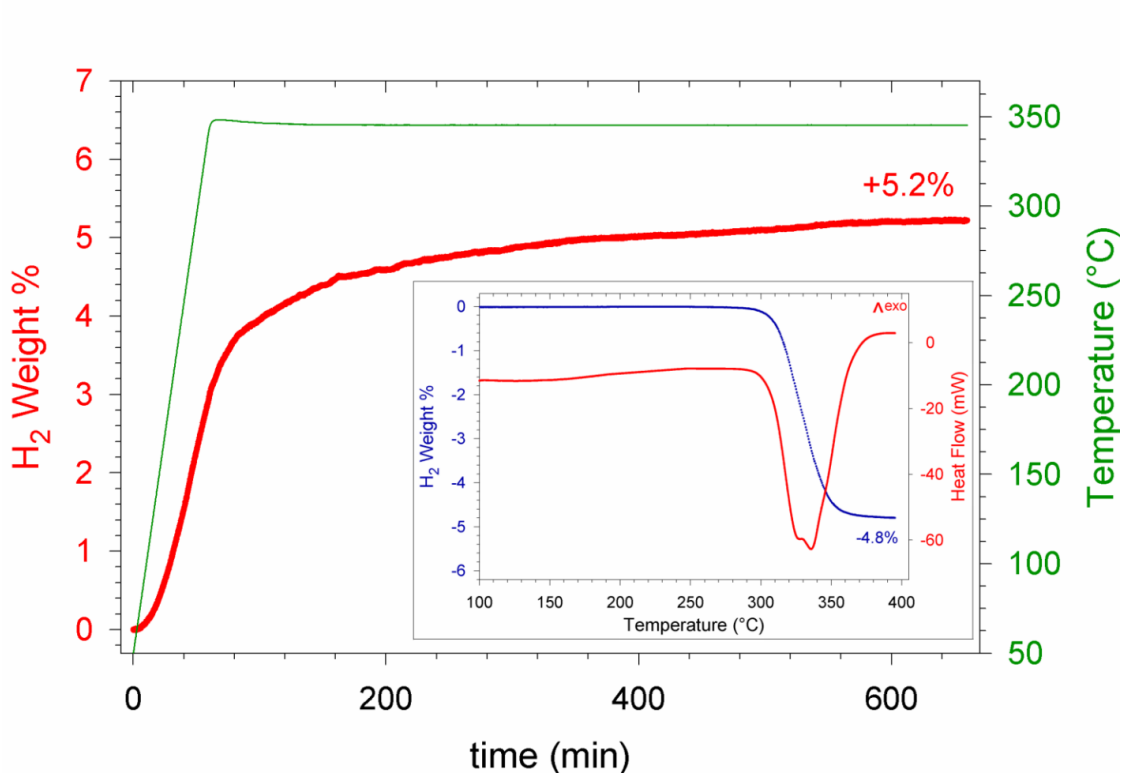

Figure 5: Kinetic absorption curve for the sample B1, obtained from the decomposition of $[NBu_4]_2^+[Ni_6(CO)_{12}]^{2-}$ metal-carbonyl cluster (thick line). The temperature ramp profile is also reported (thin line). The inset reports the coupled manometric–calorimetric desorption profiles.

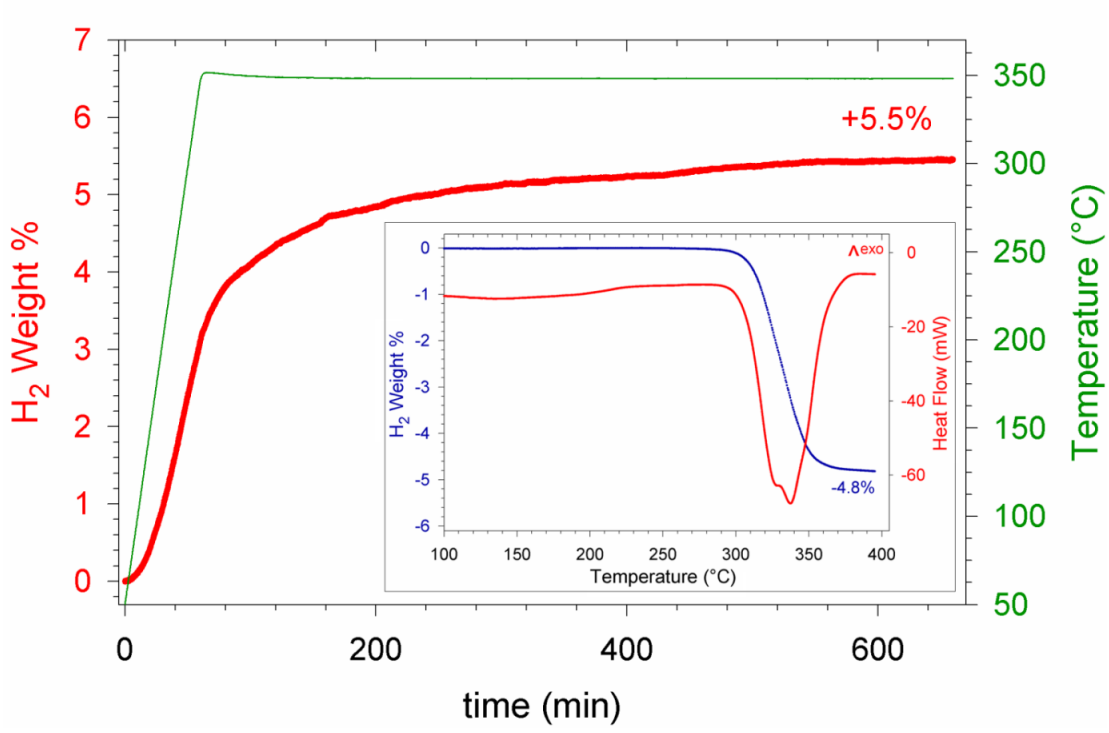

Figure 6: Kinetic absorption curve for the sample B2, obtained from the decomposition of $[NEt_4]_3^+[HNi_{12}(CO)_{21}]^{3-}$ metal-carbonyl cluster (thick line). The temperature ramp profile is also reported (thin line). The inset reports the coupled manometric–calorimetric desorption profiles.

By coupled manometric - DSC measurements (see insets in figures 5 and 6) it was possible to **demonstrate the reversibility of the hydrogenation – dehydrogenation processes (5 wt % is released after only 80 min of measurements during heating in ramp mode). Moreover, it is possible to** notice that the onset temperature for dehydrogenation process sets at 307°C for both compounds, in agreement with measurements on pure Li_6C_{60}, where the onset is found at 306°C [33].

Main desorption peaks are at 336°C and 326°C, similarly to the behavior of $Li_6Ni_{0.1}C_{60}$ obtained from nickel chloride. The related desorption enthalpy, obtained from profile integration, is 61 kJ/mol for the sample B1 and 57.3 kJ/mol for the sample B2.

3.2.2 Powder X-Ray diffraction

Nickel carbonyl clusters present very poor thermal stability: they are known to decompose at relatively low temperatures, around 150°C [34]. Hydrogenation treatment heats the sample beyond this value. X-rays diffraction was performed either on as-prepared samples, or on H_2 treated samples, and the results are shown in Figure 7.

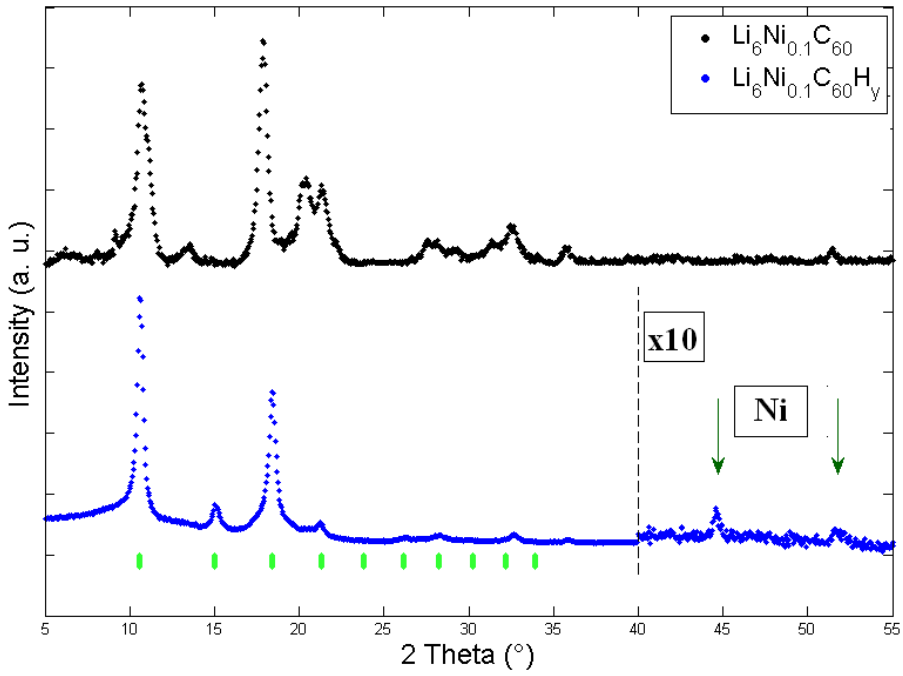

Figure 7: PXRD profile of sample B1 in pristine conditions (upper dots) and after hydrogenation (lower dots). Data collected on B2 sample are similar and are not shown. Thick marks report the reflection angle of hydrogenated fullerides (*bcc* structure with lattice parameter 11.80 Å, space group $Im\bar{3}m$), the arrows highlight the peaks of nickel in the higher 2θ region (10x magnification).

The pattern of the as prepared sample (upper black dots) is close to the one of Li_6C_{60}, which accounts for the most intense peaks. Peaks of the main phase appear broad, but they can be easily indexed with an *fcc* (space group $Fm\bar{3}m$) monomer phase expected for this compound.
As in the other synthesis, a small fraction of the sample can be attributed to the monoclinic phase isostructural to the Li_4C_{60} polymer [47].
Upon hydrogen treatment (lower blue dots in figure 7), the majority of the sample takes the hydrofullerene $C_{60}H_y$ *bcc* crystalline arrangement (lattice parameter = 11.80(4) Å, space group $Im\bar{3}m$, green thick marks in the picture). At higher angles, two weak and broad reflections, respectively at 2θ = 44.50° and 51.85°, indicate the presence of nickel metal phase, which is released during the thermal treatment, confirming the expected decomposition of the carbonyl clusters.

3.2.3 Scanning Transmission Electron Microscopy

STEM confirmed the Ni particles formation in samples B1 and B2. Pictures shown in panels a and c in Figure 8 demonstrate that nickel metal has been released by carbonyl cages and aggregated or re-crystallized during the absorption process in both compounds. In the sample B1 (obtained from Ni_6 cluster decomposition), around 210 particles were analyzed and their distribution is reported in the upper histogram in Figure 8 (panel a), while for the sample B2 (obtained from Ni_{12} cluster), around 75 were studied and the result is shown in the lower histogram (panel d).
In the former sample, particles from 2 nm up to 50 nm were mainly detected, with some particles reaching 100 nm size. In the latter, the distribution ranges from 2 nm up to 40 nm and only one particle has been found with a larger size (170 nm). A statistical study on the detected objects suggests, in both cases, a logarithmic-normal distribution [48] which is commonly used to describe the formation of particles produced through fragmentation [49].
In the sample B1, the mean value is 1.85 nm and its standard deviation σ=0.86 nm; in the sample B2, the mean value is 2.09 nm and the related standard deviation σ=0.74 nm.

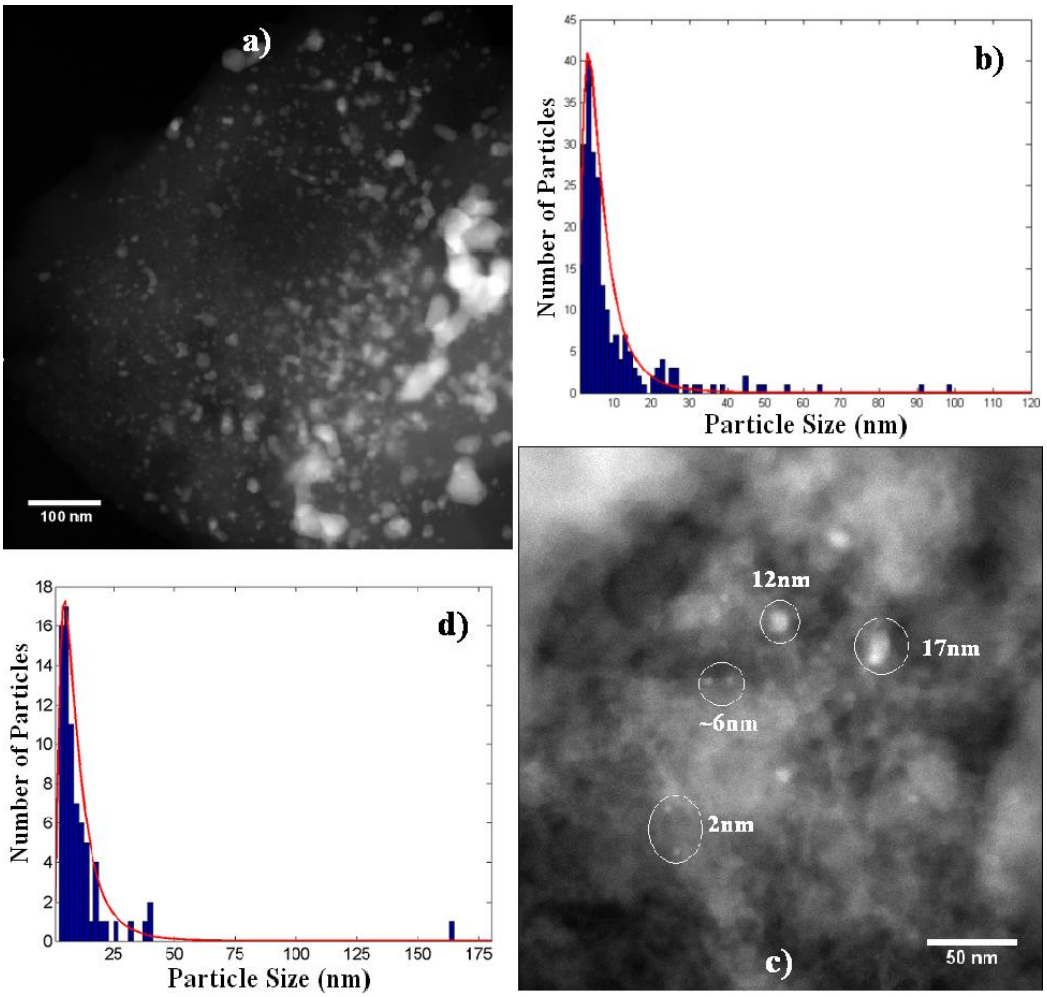

Figure 8: HAADF-STEM picture of sample B1 and B2 (panels a and c, respectively) after the hydrogenation process and particle size distribution (panel b and d for Ni_6 and Ni_{12} clusters respectively; the solid line highlights the fitting of the lognormal distribution).

3.3 Discussion

Carbon fullerene is in principle a promising material for solid-state hydrogen storage applications, as it can be easily hydrogenated [50], although the C-H binding energy overwhelms the ideal value for applications, where reversible storage is needed. The charge transfer achieved with the intercalation of alkali metal clusters promotes the formation of ionic systems, in which the hydrogenation process becomes reversible and with reasonably low desorption temperatures [24-26]. Here we found that the performance of these materials can be further improved with the introduction of nanosized transition metal particles. In fact, their high surface is able to catalyze H_2dissociation and hence to enhance the hydrogen storage properties [33].

The presence of surface catalytic effects on the hydrogen molecule dissociation in Ni nanoparticles is a long time discussed phenomenon [51-53] and its size-dependent efficiency is well known on carbon nanostructures [54]. We demonstrated that in all the three prepared samples, Ni metal has been efficiently intercalated.

In the sample A, synthesized starting from nickel chloride, the available Ni surface provides a clear enhancement of the absorption properties with respect to the pure compound, as shown in Figure 1. An even more efficient metal decoration is achieved in the second couple of compounds, samples B1 and B2, where the use of carbonyl clusters allowed the dispersion of nanometer sized Ni clusters. Also in this case, the catalytic effect of Ni enhanced the hydrogen chemical absorption with respect to pure Li_6C_{60} intercalated fullerides. In both cases, PXRD demonstrated that hydrogen is stored on the charged fullerene molecules, converting the material crystalline arrangement to *bcc*, as commonly observed in hydrofullerenes [26], and no traces of metal hydrides were detected.

Concerning the desorption process, a two-steps desorption phenomenon is met in the manometric curves in the three cases: for temperatures higher than 300°C the thermal destabilization of C-H binding is reached and the material reversibly returns to the pristine intercalated fulleride structure. The presence of two steps in the desorption process for Ni added Li_6C_{60} compounds could be ascribable either to the not perfectly homogeneous powder grain dimension of samples, or to the well-known not trivial hydrogenation/de-hydrogenation mechanism of the C_{60} units [28, 55, 56] and it is currently under investigation.

The measured de-hydrogenation enthalpies seems to correlate well with the TM particle size distribution: in the sample A, where a broader Ni particle size distribution is present (ranging from few nm to micron size), a desorption enthalpy similar to that of pure Li_6C_{60} fulleride is detected [33]. On the other hand, in samples B1 and B2, characterized by narrower particle size distributions, a noticeable reduction of de-H_2 enthalpy was found: down to 61 kJ/mol in sample B1, where σ = 0.86 nm, and even down to 57 kJ/mol in sample B2, where σ = 0.74 nm. Although the desorption enthalpy reduction is small (around 10% if compared with that of pristine Li_6C_{60}), the $Li_6Ni_{0.1}C_{60}$ compound synthesized from metal carbonyl clusters provides a proof of an efficient destabilization of hydrofullerene molecule.

As compared with Pt/Pd added Li_6C_{60} compounds, the enhancement of the absorption properties in Ni added Li_6C_{60} systems is slightly lower [33]; nevertheless, the larger availability of Ni in nature and the much more favorable price would probably justify its use as catalyst for large scale applications.

The de-hydrogenation results can be interpreted if one **considers** that both the intercalated Li clusters and the TM surfaces concur to catalyze the hydrogen desorption from the C_{60} cages.

When Ni aggregates are present (as in the synthesis from the metal chloride), they do not contribute to the desorption, probably as a consequence of their relatively low surface/volume ratio and low dispersion, and hence the desorption process is accomplished by lithium clusters only, thus explaining the same DSC behavior observed in pure Li_6C_{60} and in the sample A.

On the other hand, when a higher surface/volume ratio is obtained through the reduction of the particle size, a more intimate contact between the hydrofullerene molecules and the transition metal fraction is obtained. As a consequence of Ni surface contribution, a destabilization of C-H bonding during the desorption process is observed and the energy exchange needed to extract chemically-absorbed hydrogen is thus lowered. Such a feature, which was not achieved in the previous literature on decoration of other TMs [33], shows an alternative strategy to modify and control the desorption mechanism in the class of fullerides, besides the alkali substitution in the Li cluster [55], on the side of final uptake value, already fulfill U.S.-DoE2025 target [57]. We can therefore conclude that the particle size of Ni clusters drives the desorption behavior of the material, thus providing the possible direction to bring intercalated fullerides into the hydrogen binding energy suitable for on-board application.

4. Conclusions

Nickel addition to lithium intercalated fullerides has been realized following two different methods, which introduce a heterogeneous catalysis attributed to TM particles enhancing hydrogen storage properties. Hydrogenation and de-hydrogenation properties have been investigated showing that these materials have final gravimetric density around 5.5 wt% H_2, value that increases by 10% the absorption value of the solely intercalated alkali-metal fullerides and approaches the U.S.-DoE 2025 targets. X-rays diffraction shows the formation of the hydrofulleride C_{60}-H_y, indicating the H_2 chemical absorption on fullerene molecules as the main storage process in these systems.

The particle size reduction to the nanometer scale, demonstrated with transmission electron microscopy, is achieved by adoption of metal-carbonyl molecular clusters as source of Ni metal and provides a clear modification of hydrogen desorption enthalpy.

The proximity of the absorption values to the targets of an hydrogen based economy, the scalability of the preparation process and the possibility to tune their absorption enthalpy show that these materials, although requiring further efforts for their optimization, can be promising candidate for large scale application in the field of H_2 storage.

Acknowledgments

This work received financial support by Cariplo Fundation (Project number 2013-0592, “Carbon based nanostructures for innovative hydrogen storage systems”).

Supporting Information Available

EDS spectra of sample A after the hydrogenation process. This material is available free of charge.

References

[1] M. Momirlan, T.N. Veziroglu, Current status of hydrogen energy, Renewable and Sustainable Energy Reviews, 6 (2002) 141-179.

[2] L. Schlapbach, A. Züttel, Hydrogen-storage materials for mobile applications, Materials for Sustainable Energy, Co-Published with Macmillan Publishers Ltd, UK, 2010, pp. 265-270.

[3] B. Brousse, B. Ratier, A. Moliton, Vapor deposited solar cells based on heterojunction or interpenetrating networks of zinc phthalocyanine and C60, Thin Solid Films, 451-452 (2004) 81-85.

[4] R. Raccichini, A. Varzi, S. Passerini, B. Scrosati, The role of graphene for electrochemical energy storage, Nature Materials, 14 (2014) 271.

[5] D. Pontiroli, M. Aramini, M. Gaboardi, M. Mazzani, A. Gorreri, M. Riccò, et al., Ionic conductivity in the Mg intercalated fullerene polymer Mg_2C_{60}, Carbon, 51 (2013) 143-147.

[6] S. Scaravonati, G. Magnani, M. Gaboardi, G. Allodi, M. Riccò, D. Pontiroli, Electrochemical intercalation of fullerene and hydrofullerene with sodium, Carbon, 130 (2018) 11-18.

[7] D. Pontiroli, S. Scaravonati, G. Magnani, L. Fornasini, D. Bersani, G. Bertoni, et al., Super-activated biochar from poultry litter for high-performance supercapacitors, Microporous and Mesoporous Materials, 285 (2019) 161-169.

[8] M. Riccò, M. Belli, M. Mazzani, D. Pontiroli, D. Quintavalle, A. Jánossy, et al., Superionic Conductivity in the Li_4C_{60} Fulleride Polymer, Physical Review Letters, 102 (2009) 145901.

[9] C. Wang, M. Waje, X. Wang, J.M. Tang, R.C. Haddon, Yan, Proton Exchange Membrane Fuel Cells with Carbon Nanotube Based Electrodes, Nano Letters, 4 (2004) 345-348.

[10] R. Ströbel, J. Garche, P.T. Moseley, L. Jörissen, G. Wolf, Hydrogen storage by carbon materials, Journal of Power Sources, 159 (2006) 781-801.

[11] M.G. Nijkamp, J.E.M.J. Raaymakers, A.J. van Dillen, K.P. de Jong, Hydrogen storage using physisorption – materials demands, Applied Physics A, 72 (2001) 619-623.

[12] H. Lee, J. Ihm, M.L. Cohen, S.G. Louie, Calcium-Decorated Graphene-Based Nanostructures for Hydrogen Storage, Nano Letters, 10 (2010) 793-798.
[13] M. Gaboardi, A. Bliersbach, G. Bertoni, M. Aramini, G. Vlahopoulou, D. Pontiroli, et al., Decoration of graphene with nickel nanoparticles: study of the interaction with hydrogen, Journal of Materials Chemistry A, 2 (2014) 1039-1046.
[14] D.C. Elias, R.R. Nair, T.M.G. Mohiuddin, S.V. Morozov, P. Blake, M.P. Halsall, et al., Control of Graphene's Properties by Reversible Hydrogenation: Evidence for Graphane, Science, 323 (2009) 610.
[15] D. Pontiroli, M. Aramini, M. Gaboardi, M. Mazzani, S. Sanna, F. Caracciolo, et al., Tracking the Hydrogen Motion in Defective Graphene, The Journal of Physical Chemistry C, 118 (2014) 7110-7116.
[16] C. Cavallari, D. Pontiroli, M. Jiménez-Ruiz, M. Johnson, M. Aramini, M. Gaboardi, et al., Hydrogen motions in defective graphene: the role of surface defects, Physical Chemistry Chemical Physics, 18 (2016) 24820-24824.
[17] X.M. Liu, Y. Tang, E.S. Xu, T.C. Fitzgibbons, G.S. Larsen, H.R. Gutierrez, et al., Evidence for Ambient-Temperature Reversible Catalytic Hydrogenation in Pt-doped Carbons, Nano Letters, 13 (2013) 137-141.
[18] H. Cheng, A.C. Cooper, G.P. Pez, M.K. Kostov, P. Piotrowski, S.J. Stuart, Molecular Dynamics Simulations on the Effects of Diameter and Chirality on Hydrogen Adsorption in Single Walled Carbon Nanotubes, The Journal of Physical Chemistry B, 109 (2005) 3780-3786.
[19] M. Yoon, S. Yang, E. Wang, Z. Zhang, Charged Fullerenes as High-Capacity Hydrogen Storage Media, Nano Letters, 7 (2007) 2578-2583.
[20] Q. Sun, P. Jena, Q. Wang, M. Marquez, First-Principles Study of Hydrogen Storage on $Li_{12}C_{60}$, Journal of the American Chemical Society, 128 (2006) 9741-9745.
[21] G.J. Kubas, Metal–dihydrogen and σ-bond coordination: the consummate extension of the Dewar–Chatt–Duncanson model for metal–olefin π bonding, Journal of Organometallic Chemistry, 635 (2001) 37-68.
[22] T. Yildirim, O. Zhou, J.E. Fischer, N. Bykovetz, R.A. Strongin, M.A. Cichy, et al., Intercalation of sodium heteroclusters into the C_{60} lattice, Nature, 360 (1992) 568.
[23] F. Giglio, D. Pontiroli, M. Gaboardi, M. Aramini, C. Cavallari, M. Brunelli, et al., $Li_{12}C_{60}$: A lithium clusters intercalated fulleride, Chemical Physics Letters, 609 (2014) 155-160.
[24] J.A. Teprovich, M.S. Wellons, R. Lascola, S.-J. Hwang, P.A. Ward, R.N. Compton, et al., Synthesis and Characterization of a Lithium-Doped Fullerane (Lix-C_{60}-Hy) for Reversible Hydrogen Storage, Nano Letters, 12 (2012) 582-589.

[25] P. Mauron, M. Gaboardi, A. Remhof, A. Bliersbach, D. Sheptyakov, M. Aramini, et al., Hydrogen Sorption in $Li_{12}C_{60}$, The Journal of Physical Chemistry C, 117 (2013) 22598-22602.
[26] P. Mauron, A. Remhof, A. Bliersbach, A. Borgschulte, A. Züttel, D. Sheptyakov, et al., Reversible hydrogen absorption in sodium intercalated fullerenes, International Journal of Hydrogen Energy, 37 (2012) 14307-14314.
[27] P. Mauron, M. Gaboardi, D. Pontiroli, A. Remhof, M. Riccò, A. Züttel, Hydrogen Desorption Kinetics in Metal Intercalated Fullerides, The Journal of Physical Chemistry C, 119 (2015) 1714-1719.
[28] M. Gaboardi, S. Duyker, C. Milanese, G. Magnani, V.K. Peterson, D. Pontiroli, et al., In Situ Neutron Powder Diffraction of Li_6C_{60} for Hydrogen Storage, The Journal of Physical Chemistry C, 119 (2015) 19715-19721.
[29] D. Pontiroli, D. D'Alessio, M. Gaboardi, G. Magnani, C. Milanese, S.G. Duyker, et al., Ammonia-storage in lithium intercalated fullerides, Journal of Materials Chemistry A, 3 (2015) 21099-21105.
[30] M. Aramini, M. Gaboardi, G. Vlahopoulou, D. Pontiroli, C. Cavallari, C. Milanese, et al., Muon spin relaxation reveals the hydrogen storage mechanism in light alkali metal fullerides, Carbon, 67 (2014) 92-97.
[31] M. Gaboardi, C. Cavallari, G. Magnani, D. Pontiroli, S. Rols, M. Riccò, Hydrogen storage mechanism and lithium dynamics in $Li_{12}C_{60}$ investigated by μSR, Carbon, 90 (2015) 130-137.
[32] M. Pozzo, D. Alfè, Hydrogen dissociation and diffusion on transition metal (=Ti, Zr, V, Fe, Ru, Co, Rh, Ni, Pd, Cu, Ag)-doped Mg(0001) surfaces, International Journal of Hydrogen Energy, 34 (2009) 1922-1930.
[33] M. Aramini, C. Milanese, D. Pontiroli, M. Gaboardi, A. Girella, G. Bertoni, et al., Addition of transition metals to lithium intercalated fullerides enhances hydrogen storage properties, International Journal of Hydrogen Energy, 39 (2014) 2124-2131.
[34] G. Longoni, P. Chini, A. Cavalieri, Carbonylnickelates. 1. Synthesis and chemical characterization of the dodecacarbonylpentanickelate(2-) and dodecacarbonylhexanickelate(2-) dianions, Inorganic Chemistry, 15 (1976) 3025-3029.
[35] M. Gaboardi, N. Sarzi Amadè, M. Riccò, C. Milanese, A. Girella, M. Gioventù, et al., Synthesis and characterization of mixed sodium and lithium fullerides for hydrogen storage, International Journal of Hydrogen Energy, 43 (2018) 16766-16773.
[36] N. Bergemann, C. Pistidda, C. Milanese, M. Aramini, S. Huotari, P. Nolis, et al., A hydride composite featuring mutual destabilisation and reversible boron exchange: $Ca(BH_4)_2$–Mg_2NiH_4, Journal of Materials Chemistry A, 6 (2018) 17929-17946.

[37] J. Jepsen, C. Milanese, J. Puszkiel, A. Girella, B. Schiavo, G.A. Lozano, et al., Fundamental Material Properties of the 2LiBH4-MgH2 Reactive Hydride Composite for Hydrogen Storage: (I) Thermodynamic and Heat Transfer Properties, Energies, 11 (2018) 1081.

[38] M. Zieliński, R. Wojcieszak, S. Monteverdi, M. Mercy, M.M. Bettahar, Hydrogen storage in nickel catalysts supported on activated carbon, International Journal of Hydrogen Energy, 32 (2007) 1024-1032.

[39] A.K. Singh, M.A. Ribas, B.I. Yakobson, H-Spillover through the Catalyst Saturation: An Ab Initio Thermodynamics Study, ACS Nano, 3 (2009) 1657-1662.

[40] Y.-J. Han, S.-J. Park, Influence of nickel nanoparticles on hydrogen storage behaviors of MWCNTs, Applied Surface Science, 415 (2017) 85-89.

[41] C. Cavallari, S. Rols, H.E. Fischer, M. Brunelli, M. Gaboardi, G. Magnani, et al., Neutron scattering study of nickel decorated thermally exfoliated graphite oxide, International Journal of Hydrogen Energy, 44 (2019) 30999-31007.

[42] M. Riccò, M. Belli, D. Pontiroli, M. Mazzani, T. Shiroka, D. Arčon, et al., Recovering metallicity in A_4C_{60}: The case of monomeric Li_4C_{60}, Physical Review B, 75 (2007) 081401.

[43] L. Maidich, D. Pontiroli, M. Gaboardi, S. Lenti, G. Magnani, G. Riva, et al., Investigation of Li and H dynamics in Li_6C_{60} and $Li_6C_{60}H_y$, Carbon, 96 (2016) 276-284.

[44] M. Riccò, T. Shiroka, M. Belli, D. Pontiroli, M. Pagliari, G. Ruani, et al., Unusual polymerization in the Li_4C_{60} fulleride, Physical Review B, 72 (2005) 155437.

[45] A.M. Molodets, A.S. Lobach, A.N. Zhukov, Y.M. Shulga, V.E. Fortov, Stability of crystalline structure and molecules of hydrofullerene $C_{60}H_{36}$ under high shock pressures, Doklady Physics, 53 (2008) 562-565.

[46] S.R. Stopić, I.B. Ilić, D.P. Uskoković, Effect of Pd, Cu, and Ni additions on the kinetics of $NiCl_2$ reduction by hydrogen, Metallurgical and Materials Transactions B, 28 (1997) 1241-1248.

[47] S. Margadonna, D. Pontiroli, M. Belli, T. Shiroka, M. Riccò, M. Brunelli, Li_4C_{60}: A Polymeric Fulleride with a Two-Dimensional Architecture and Mixed Interfullerene Bonding Motifs, Journal of the American Chemical Society, 126 (2004) 15032-15033.

[48] B. Epstein, The mathematical description of certain breakage mechanisms leading to the logarithmico-normal distribution, Journal of the Franklin Institute, 244 (1947) 471-477.

[49] Z. Cheng, S. Redner, Kinetics of fragmentation, Journal of Physics A: Mathematical and General, 23 (1990) 1233.

[50] A.V. Talyzin, Y.M. Shulga, A. Jacob, Comparative study of hydrofullerides $C_{60}H_x$ synthesized by direct and catalytic hydrogenation, Applied Physics A, 78 (2004) 1005-1010.

[51] L.H. Germer, A.U. MacRae, Adsorption of Hydrogen on a (110) Nickel Surface, The Journal of Chemical Physics, 37 (1962) 1382-1386.
[52] S.M. Foiles, M.I. Baskes, C.F. Melius, M.S. Daw, Calculation of hydrogen dissociation pathways on nickel using the embedded atom method, Journal of the Less Common Metals, 130 (1987) 465-473.
[53] A.V. Hamza, R.J. Madix, Dynamics of the dissociative adsorption of hydrogen on nickel(100), The Journal of Physical Chemistry, 89 (1985) 5381-5386.
[54] L. Yang, C. Xie, C. Hu, M. Zheng, H. Wang, J. Cui, et al., Effects of Ni Particle Size on Hydrogen Storage of Ni-Doped High Surface Area Activated Carbon, Australian Journal of Chemistry, 66 (2013) 548-554.
[55] M. Gaboardi, C. Milanese, G. Magnani, A. Girella, D. Pontiroli, P. Cofrancesco, et al., Optimal hydrogen storage in sodium substituted lithium fullerides, Physical Chemistry Chemical Physics, 19 (2017) 21980-21986.
[56] M. Gaboardi, N. Sarzi Amadé, M. Aramini, C. Milanese, G. Magnani, S. Sanna, et al., Extending the hydrogen storage limit in fullerene, Carbon, 120 (2017) 77-82.
[57] U.S DOE Annual energy outlook. Available online at: https://www.energy.gov/eere/fuelcells/doe-technical-targets-onboard-hydrogen-storage-light-duty-vehicles